ReaxFF$_{SiO}$ Reactive Force Field for Silicon and Silicon Oxide Systems

Adri C. T. van Duin,[†] Alejandro Strachan,[‡] Shannon Stewman,[‡] Qingsong Zhang,[‡] Xin Xu,[‡] and William A. Goddard, III*,[‡]

Department of Fossil Fuels and Environmental Geochemistry, Drummond Building, University of Newcastle, Newcastle upon Tyne NE1 7RU, United Kingdom, and Materials and Process Simulation Center, Beckman Institute (139-74), Division of Chemistry and Chemical Engineering, California Institute of Technology, Pasadena, California 91125

Received: December 5, 2002

To predict the structures, properties, and chemistry of materials involving silicon and silicon oxides; interfaces between these materials; and hydrolysis of such systems, we have developed the ReaxFF$_{SiO}$, reactive force field. The parameters for this force field were obtained from fitting to the results of quantum chemical (QC) calculations on the structures and energy barriers for a number of silicon oxide clusters and on the equations of state for condensed phases of Si and SiO_2 from QC. We expect that ReaxFF$_{SiO}$ will allow accurate dynamical simulations of bond breaking processes in large silicon and silicon oxide systems. ReaxFF$_{SiO}$ is based closely on the potential functions of the ReaxFF$_{CH}$ reactive force field for hydrocarbons, so that it should also be useful for describing reactions of organics with Si and SiO_2 systems.

1. Introduction

Information about the atomic level detail at interfaces between dissimilar materials is often critical for developing new and improved materials and devices, but all too often, it is difficult to obtain such information from experiment. Thus, it is important to use theory and computation to elicit the structures and properties of such interfaces. Because the spatial scales are often far too large for quantum mechanics, it would be useful to have force fields (FFs) that accurately describe structures, properties, and chemical processes associated with interfaces. Because the structures at these interfaces may differ substantially from either parent phase, it is essential that the FF is capable of describing all possible environments and that it allow the structure to evolve from any particular guess to the final optimum structures. Ideally, the FF would describe the reactions used to synthesize the interface because the actual structure may be determined by the kinetics.

A number of empirical FFs have been developed for silicon oxides and related structures.[1−9] These FFs have been successful in providing valuable insight into the structures[10,11] and have been used to simulate interactions of silicon oxides with organic compounds.[12,13] However, such empirical FFs are generally reliable only near equilibrium with fixed bond orders and fixed charges designed specifically for a limited range of silicon oxide morphologies, reducing the transferability to new structures. Improvements lifting some of these restrictions include allowing charges to migrate in the dynamics (charge equilibration QEq[9,14] or EEM[5,15]) and replacing rigid bond energy and bond angle terms with more versatile potential functions applicable to a range of Si and O coordinations.[5] However, such approaches have not been systematically introduced into FF describing reactions.

We present here a new generation of force field (the Reactive Force Field, ReaxFF$_{SiO}$) that aims at providing a consistent description appropriate for both covalent systems (crystalline Si) and all forms of silicon oxides (including the high pressure 6-coordinate Stishovite phase and low-density zeolites) and capable of describing the reactions between the covalent and ionic limits to describe the interfaces between these phases. The development strategy for ReaxFF$_{SiO}$ closely follows that of the reactive force field for hydrocarbons[16] (ReaxFF$_{CH}$). All parameters are determined from QC calculations (no empirical data is used) making it a first-principles FF.

The QC test set used to derive the ReaxFF$_{SiO}$ parameters includes the following: a variety of SiO-clusters to test the capability of the force field for describing a variety of equilibrium structures and for describing the continuous dissociation of various bonds; crystalline phases with all known coordinations (4 and 6 for bulk Si, 4 and 6 for SiO_2) in a wide volume range, including pressures up to 500 GPa in compression and −10 GPa in tension.

ReaxFF$_{SiO}$ allows practical molecular dynamics studies of reactive systems combining silicon and silicon oxide, providing the means to characterize the chemistry and structures at their interfaces. We expect that it will be possible to extend these methods, so that reactive force fields might eventually capture the reactivity for the remainder of the periodic table.

2. Force Field

The potential functions in ReaxFF$_{SiO}$ are the same as those used in ReaxFF$_{CH}$,[16] with just a few exceptions as described below. Thus, we will describe here just the general concepts of common aspects of ReaxFF, with a more detailed discussion only of the exceptions. The system energy is partitioned into the several partial energy contributions in eq 1

$$E_{system} = E_{bond} + E_{over} + E_{under} + E_{lp} + E_{val} + E_{pen} + E_{tors} + E_{conj} + E_{vdWaals} + E_{Coulomb} \quad (1)$$

A fundamental difference between ReaxFF and most other force fields is that ReaxFF does not use fixed connectivity

* To whom correspondence should be addressed.
[†] University of Newcastle.
[‡] California Institute of Technology.

10.1021/jp0276303 CCC: $25.00
Published on Web 04/23/2003

assignments for the chemical bonds. Instead the bond order, BO′, is calculated directly from the instantaneous interatomic distances r_{ij} (eq 2), which are updated continuously. This allows for the creation and dissociation of bonds during a simulation. The bond energy (E_{bond}) is determined solely from BO as in eq 3

$$\mathrm{BO}'_{ij} = \mathrm{BO}'^{\sigma}_{ij} + \mathrm{BO}'^{\pi}_{ij} + \mathrm{BO}'^{\pi\pi}_{ij} = \exp\left[p_{\mathrm{bo},1}\left(\frac{r_{ij}}{r_0^{\sigma}}\right)^{p_{\mathrm{bo},2}}\right] + \exp\left[p_{\mathrm{bo},3}\left(\frac{r_{ij}}{r_0^{\pi}}\right)^{p_{\mathrm{bo},4}}\right] + \exp\left[p_{bo,5}\left(\frac{r_{ij}}{r_0^{\pi\pi}}\right)^{p_{\mathrm{bo},6}}\right] \quad (2)$$

Furthermore, all other covalent interactions (e.g., the functions describing bond angles and torsion angles, E_{val} and E_{tors}) are expressed in terms of these bond orders so that all terms dissociate properly as any bond is broken. This ensures that all partial energy contributions associated with valence interactions disappear smoothly upon dissociation of any of the bonds making up the valence or torsion angle.

Because bonds are breaking and reforming during dynamics, we cannot exclude Coulomb and van der Waals interactions for bonded atoms as commonly done in many FF. Instead, we must include these pairwise nonbond interactions between every atom pair, independent of the instantaneous connectivity. This is very natural for the coulomb interactions because QEq treats the atomic charges as having the finite size of the atom, leading to shielding of the Coulomb interaction for shorter distances. We also include a similar shielding for van der Waals interactions between close atoms.

To extend ReaxFF$_{\text{CH}}$ to silicon oxides, we made three additions to the ReaxFF$_{\text{CH}}$ potential functions.

2.1. Bond Energy Function. Both ReaxFF$_{\text{CH}}$ and ReaxFF$_{\text{SiO}}$ allow separate functional forms (BO^{σ}, BO^{π}, and $\mathrm{BO}^{\pi\pi}$) to describe single, double, and triple bonds. Each of these BOs have a different dependence on bond distance with the parameters determined from calculations on molecules such as $H_3Si-SiH_3$, $H_2Si{=}SiH_2$, H_3Si-OH, and $H_2Si{=}O$. However, in ReaxFF$_{\text{CH}}$, the bond energy is a function of the total bond order ($\mathrm{BO}^{\sigma} + \mathrm{BO}^{\pi} + \mathrm{BO}^{\pi\pi}$), whereas ReaxFF$_{\text{SiO}}$ uses separate dissociation energies for single, double, and triple bonds, as in eq 3. The reason for this is that, although carbon−carbon systems have bond energies that increase systematically for single to double to triple bonds (dissociation energies of 98, 178, and 235 kcal/mol), we find that Si or O containing bonds have very different behaviors (e.g., the $H_2Si{=}SiH_2$ bond is weaker than the $H_3Si-SiH_3$ bond).

To employ three bond dissociation energies, the total bond order is partitioned into contributions from sigma-bonds, pi-bonds, and double pi-bonds (triple bonds), as indicated in eq 2. As in ReaxFF$_{\text{CH}}$, the bond orders BO′ as obtained from eq 2 are corrected for overcoordination. Using these corrected contributions (BO), eq 3 is used to calculate bond energies in ReaxFF$_{\text{SiO}}$

$$E_{\text{bond}} = -D_{\text{e}}^{\sigma}\mathrm{BO}_{ij}^{\sigma}\exp\left[p_{\mathrm{be},1}\left(1-(\mathrm{BO}_{ij}^{\sigma})^{p_{\mathrm{be},2}}\right)\right] - D_{\text{e}}^{\pi}\mathrm{BO}_{ij}^{\pi} - D_{\text{e}}^{\pi\pi}\mathrm{BO}_{ij}^{\pi\pi} \quad (3)$$

Figure 1 shows the interatomic distance dependency of the Si−Si bond order. Unlike hydrocarbon systems, formation of triple bonds is not a viable option in Si−Si systems. Thus, SiH−SiH forms a single bond not a triple bond as in HCCH, and no double pi-bond contribution is calculated for these systems.

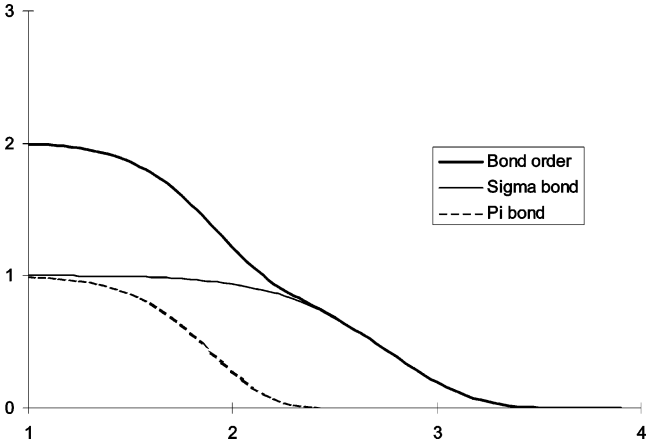

Figure 1. Dependency of the silicon−silicon bond order on interatomic distance.

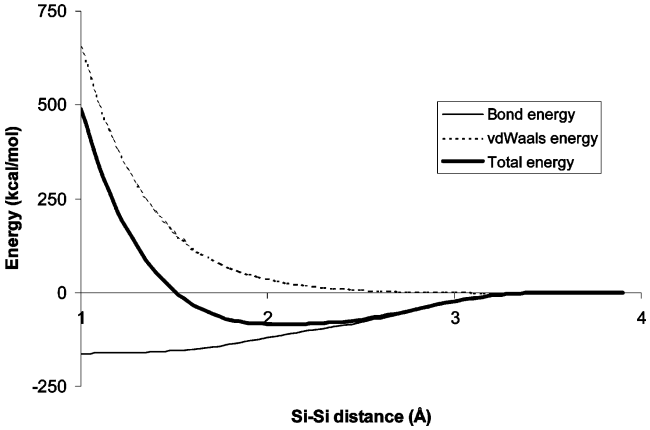

Figure 2. Dependency of the Si−Si van der Waals and bond energy terms on interatomic distance for a Si−Si diatomic. Energy effects related to under- and overcoordination are not taken into account in this plot.

Figure 2 shows the interatomic distance dependency of the van der Waals and bond energy terms in the Si−Si diatomic system.

2.2. Lone Pair Electrons. The second new potential function used in ReaxFF$_{\text{SiO}}$ is the addition of an energy term associated with lone electron pairs [E_{lp}, eq 1]. Lone electron pairs generally play little role in hydrocarbon chemistry, but lone pairs on heteroatoms such as oxygen and nitrogen can affect dramatically the response of these atoms to over- and undercoordination. Furthermore, the presence of these lone electron pairs influences the valence angles around atoms (this aspect was already incorporated in ReaxFF$_{\text{CH}}$). In addition, by delocalizing, they can contribute to the stability of conjugated systems.

Equation 4 is used to determine the number of lone pairs around an atom. Δ_i^e in eq 4 is the difference between the total number of outer shell electrons (6 for oxygen, 4 for silicon, and 1 for hydrogen) and the sum of bond orders around an atomic center

$$n_{\mathrm{lp},i} = \mathrm{int}\left(\frac{\Delta_i^e}{2}\right) + \exp\left[-\lambda_{16}\left(2 + \Delta_i^e - 2\,\mathrm{int}\left\{\frac{\Delta_i^e}{2}\right\}\right)^2\right] \quad (4)$$

For oxygen with normal coordination (total bond order = 2, $\Delta_i^e = 4$), eq 4 leads to 2 lone pairs. As the total bond order associated with a particular O starts to exceed 2, eq 4 causes a lone pair to gradually break up. This is accompanied by an energy penalty, as calculated by eq 5. $\Delta_{\mathrm{lp},i}$ in eq 5 depicts the

deviation of the number of lone pairs around an atom from the number of lone pairs at normal coordination (2 for oxygen, 0 for silicon and hydrogen)

$$E_{lp} = \frac{p_{lp}\Delta_{lp,i}}{1 + \exp(-75\Delta_{lp,i})} \quad (5)$$

To further account for the influence of lone pairs on molecular stability, the energy expressions used in ReaxFF$_{CH}$ to calculate the contributions of over-coordination energy (E_{over}) have been expanded to account for deviations in the number of lone pairs. Thus, eqs 6a−c are used in ReaxFF$_{SiO}$ to calculate the overcoordination energy

$$E_{over} = \frac{\sum_{j=1}^{nbond} p_{be,3}BO_{ij}}{\Delta_i' + Val_i}\Delta_i'\left[\frac{1}{1 + \exp(\lambda_6\Delta_i')}\right] \quad (6a)$$

$$\Delta_i' = -\Delta_{lp,i}\frac{1}{1 + \lambda_{33}\exp(\lambda_{32}SOV)} + \sum_{j=1}^{nbond} BO_{ij} - Val_i \quad (6b)$$

$$SOV = \sum_{j=1}^{neighbors(j)} (\Delta_j - \Delta_{lp,j})BO_{ij}^{\pi} \quad (6c)$$

The overcoordination for ReaxFF$_{SiO}$ differs from that for ReaxFF$_{CH}$ in that the overcoordination penalty gets diminished for systems such as $H_2C{=}N{=}N$ and R−NO2 which contain an over coordinated atom as a result of breaking up a formal lone electron pair ($\Delta_{lp,i} = 1$) next to a formally undercoordinated atom(s). For the silicon oxide systems discussed here, these modifications in the overcoordination functions have only a minor influence on the system energy. However, we expect them to be important as ReaxFF is extended to treat such atoms as nitrogen.

2.3. Valence Angle Function. The third modification involves the influence of lone pairs and undercoordination on the valence angle energy contribution. The Si atoms in the β-Si crystal (white Sn structure) are six-coordinate Si with bond angles that range from 152.7° (for a volume $V = 9.93$ Å^3 per Si) to 154.5° (for a volume $V = 17.02$ Å^3 per Si), leading to significant valence angle strain. We found that with the undercoordination expression from ReaxFF$_{CH}$ (which with symmetric expansion around a 4-coordinated atom results in modification of the equilibrium angle Θ_0) we could not reproduce the equation of state for β-Si crystal. This problem was resolved by replacing the part of the ReaxFF$_{CH}$ potential describing the influence of bond orders on Θ_0 with eq 7d. The $\Delta_{lp,j}$ in eq 7d is the deviation from the number of lone pairs calculated by eq 4. The remainder of the valence angle potential [eq 7a−c] retains the same form as in ReaxFF$_{CH}$. All of the modifications described can be incorporated in the original ReaxFF$_{CH}$ force field, and we will report later the reoptimized ReaxFF$_{CH}$ parameters

$$E_{val} = f_7(BO_{ij})\, f_7(BO_{jk})\, f_8(\Delta_j)\{k_a - k_a \exp[-k_b(\Theta_0 - \Theta_{ijk})^2]\} \quad (7a)$$

$$f_7(BO_{ij}) = 1 - \exp(-\lambda_{11}BO_{ij}^{\lambda_{12}}) \quad (7b)$$

$$f_8(\Delta_j) = \frac{2 + \exp(-\lambda_{13}\Delta_j)}{1 + \exp(-\lambda_{13}\Delta_j) + \exp(p_{v,1}\Delta_j)} \times \left[\lambda_{14} - (\lambda_{14} - 1)\frac{2 + \exp(\lambda_{15}\Delta_j)}{1 + \exp(\lambda_{15}\Delta_j) + \exp(-p_{v,2}\Delta_j)}\right] \quad (7c)$$

$$SBO = 1 - \left[\prod_{n=1}^{neighbors(j)} \exp(-BO_{jn}^{8})\right](\Delta_j - \lambda_{34}\Delta_{lp,j} + \sum_{n=1}^{neighbors(j)} BO_{jn,\pi}) \quad (7d)$$

$$SBO2 = 0 \text{ if } SBO \le 0$$

$$SBO2 = SBO^{\lambda_{17}} \text{ if } 0 < SBO < 1$$

$$SBO2 = 2 - (2 - SBO)^{\lambda_{17}} \text{ if } 1 < SBO < 2$$

$$SBO2 = 2 \text{ if } SBO > 2$$

$$\Theta_0 = \pi - \Theta_{0,0}\{1 - \exp[-\lambda_{18}(2 - SBO2)]\}$$

2.4. Computational Details. Parameter values for the potential functions (see Appendix tables) were obtained by optimization against a set of data obtained from quantum chemical (QC) methods. For the noncondensed systems, DFT simulations were performed using the Jaguar program (version 4.0) with the B3LYP functional and a 6-31G** basis set.

We also used DFT to perform QC calculations on crystalline Si and SiO_2 systems. We used the plane-wave code CASTEP[17] using the generalized gradient approximation (GGA) for the exchange-correlation potential and ultrasoft pseudopotentials to replace the core electrons. For the Si crystal calculations, we used the Perdew, Burke, and Ernzerhof (PBE) implementation of GGA[18] and a kinetic energy cutoff of 350 eV. We used the Monkhorst−Pack[19] scheme to generate the *k*-space grid, and the number of *k* points in the irreducible Brillouin zone was 28 for the 2-atom a unit cell, 120 for the 2-atom b unit cell, and 20 for the simple cubic lattice. For the SiO_2 crystals, we used the Perdew−Wang implementation of GGA,[20] a kinetic energy cutoff of 380 eV and also used the Monkhorst−Pack scheme to generate the *k*-space grid using a spacing of 0.1 Å^{-1}.

A successive one-parameter search technique[21] was used to optimize the force field.

3. Results

3.1. Bond Dissociation. To optimize the reactive force field bond energy, DFT simulations were carried out for dissociation of single and double bonds of Si−Si, Si−O, and O−O. To facilitate application of ReaxFF$_{SiO}$ to small SiO clusters, we also determined parameters for Si−H and O−H bonds. Figures 3 and 4 show the ReaxFF$_{SiO}$ data for single and double Si−Si bond dissociation in $H_3Si{-}SiH_3$ and $H_2Si{=}SiH_2$. Figures 5 and 6 show the Si−O dissociation curves for $H_3Si{-}O{-}SiH_3$ and $H_2Si{=}O$. The O−O dissociation curves were obtained for the HO−OH and molecular oxygen, whereas SiH_4 and H_2O were used to derive Si−H and O−H bond energies. Comparisons between ReaxFF$_{SiO}$ and DFT bond dissociation energies for these latter four systems are included in the Supporting Information.[22] In each case, DFT-dissociation curves were calculated for the singlet and triplet systems. To optimize the ReaxFF$_{SiO}$-parameters we used DFT for the singlet state from the equilibrium distance up to the point where it is comparable to the dissociation limit (to the lowest of either the singlet or triplet full bond dissociation energies).

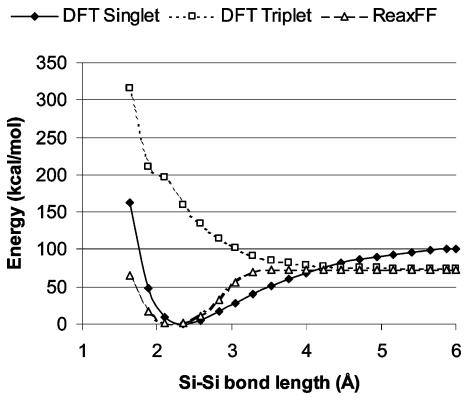

Figure 3. Dissociation of the Si−Si single bond in $H_3Si-SiH_3$.

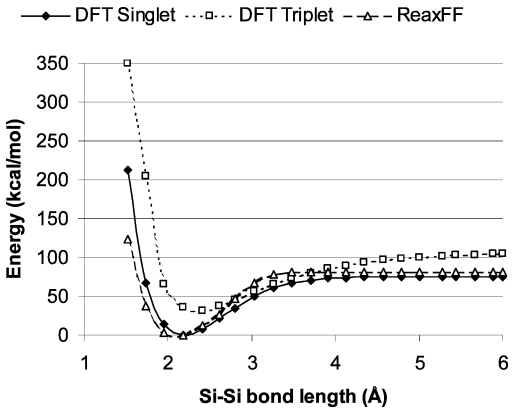

Figure 4. Dissociation of the Si−Si double bond in $H_2Si=SiH_2$.

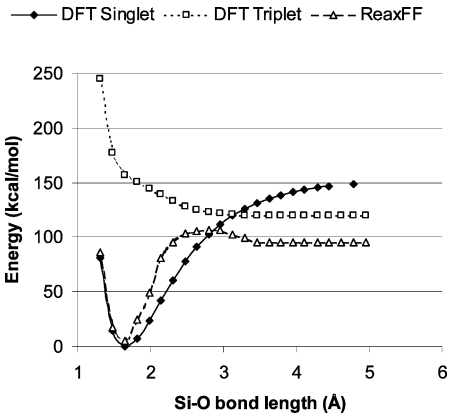

Figure 5. Dissociation of the Si−O bond in $H_3Si-O-SiH_3$.

3.2. Valence Angles Terms. To optimize the valence angle parameters for $ReaxFF_{SiO}$, we calculated angle bend energies from DFT calculations on various small clusters of silicon and silicon oxide. For HSiO systems, there are 12 different valence angle cases (X−Y−Z) (excluding Y═H). For each of these 12 valence angles, we took a representative monomer (e.g., $H_3Si-O-SiH_3$ for the Si−O−Si angle). Using DFT, the geometry of each monomer was minimized for various fixed values of the angle of interest (±31, ±17, ±9, ±5, ±3, and ±1° from the value in the relaxed structure). For each fixed valence angle, the rest of the geometry was reoptimized to obtain an adiabatic DFT valence energy curve against which the $ReaxFF_{SiO}$ parameters could be optimized. Figures 7−9 compare the $ReaxFF_{SiO}$ energies for the Si−O−Si, Si−Si−Si, and O−Si−O valence angles with the DFT data. The data for the $ReaxFF_{SiO}$ and DFT calculations on the other 9 angles are in the supplementary meterial.[22]

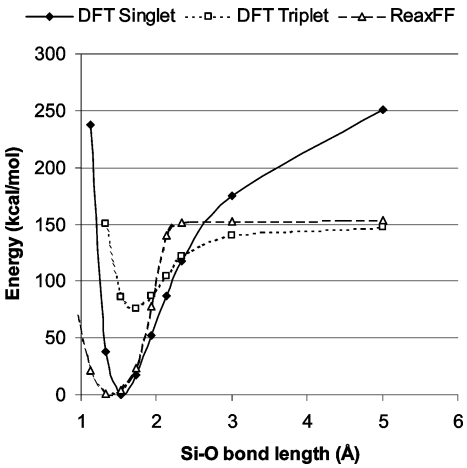

Figure 6. Dissociation of the Si−O double bond in $H_2Si=O$.

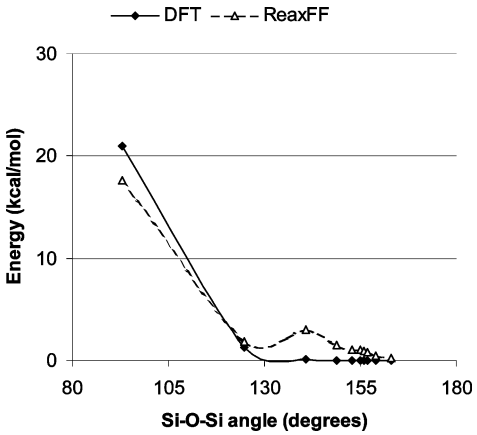

Figure 7. Adiabatic energy of $H_3Si-O-SiH_3$ as a function of the Si−O−Si valence angle.

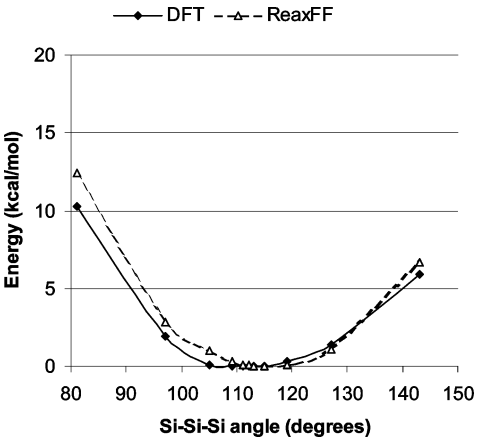

Figure 8. Adiabatic energy of $H_3Si-SiH_2-SiH_3$ as a function of the Si−Si−Si valence angle.

To further test and optimize the valence angle parameters for $ReaxFF_{SiO}$, we carried out DFT calculations on cyclic six membered rings: *c*-$(SiH_2-O)_3$ and *c*-$(SiH_2)_6$. Each ring was first minimized and subsequently distorted by modifying the distances between the molecular center of mass and three Si atoms. Figures 10 and 11 show how $ReaxFF_{SiO}$ performs in reproducing the DFT-distortion energies for these six-membered rings.

3.3. Torsion Angle Terms. To determine the $ReaxFF_{SiO}$ torsion potentials, additional DFT calculations were performed on the chair, boat, and planar conformations of *c*-$(SiH_2)_6$ (Table 1).

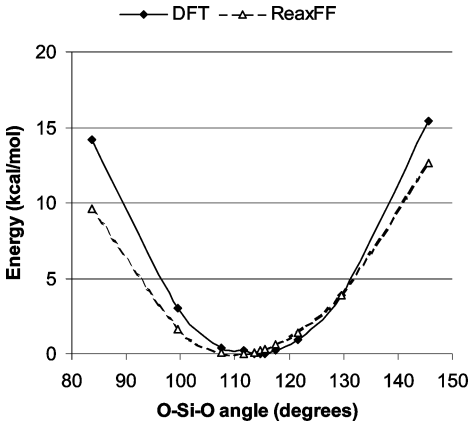

Figure 9. Adiabatic energy of HO−SiH_2−OH as a function of the O−Si−O valence angle.

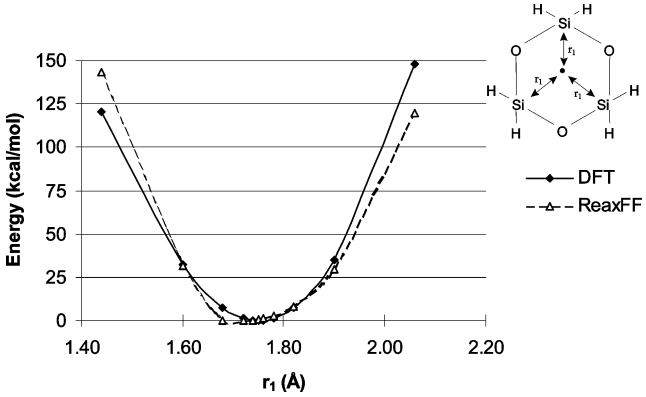

Figure 10. Distortion energies for *c*-$(SiH_2O)_3$ ring for DFT and ReaxFF$_{SiO}$.

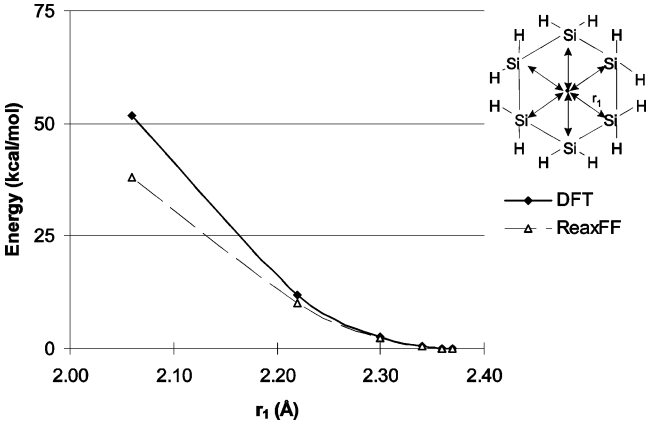

Figure 11. Distortion energies for *c*-$(SiH_2)_6$ ring for DFT and ReaxFF$_{SiO}$.

TABLE 1: DFT and ReaxFF$_{SiO}$ Conformation Energies (kcal/mol) for the *c*-$(SiH_2)_6$ Six-Membered Ring (Chair Is the Lowest Energy)

conf. 1	conf. 2	ΔE_{DFT}	ΔE_{reaxFF}
chair	boat	1.8	1.4
chair	planar	7.4	7.2

3.4. Under/Overcoordination. To provide input data from QC on the relation between bond order, coordination, and valence, we carried out DFT calculations on model compounds containing 2- and 4-coordinated oxygen atoms and on model compounds containing 4- and 6-coordinated silicon atoms. To describe oxygen overcoordination/undercoordination, we determined the reaction energy for the addition of two H_3Si groups to the oxygen atom in $H_3Si-O-SiH_3$. To describe silicon overcoordination/undercoordination, we determined the reaction energy for adding two OH groups to the silicon atom in $Si(OH)_4$; the energetics for the hydrogen shift converting $H_2Si{=}SiH_2$ to $H_3Si-SiH$; the energetics for ring opening of *c*-$(O-SiH_2-SiH_2)$ [i.e., oxygen bridged $H_2Si-SiH_2$] to form the $\bullet O-SiH_2-SiH_2\bullet$ biradical; and the energetics for ring opening of *c*-$(O-SiH_2-SiH_2)$ [i.e., oxygen bridged $H_2Si-SiH_2$] to form the $\bullet SiH_2-O-SiH_2\bullet$ biradical.

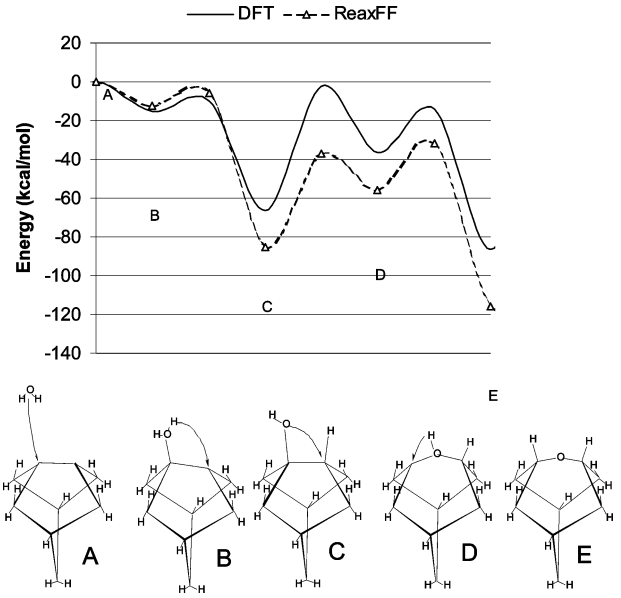

Figure 12. Reaction energy profile for the reaction of water with a Si_9H_{10}-cluster modeling the (100) surface of the α-Si crystal.

TABLE 2: Under- and Overcoordination Energetics (kcal/mol) for Oxygen and Silicon

reaction	E_{DFT}	E_{ReaxFF}
$(H_3Si)_2-O + H_3Si-SiH_3 \rightarrow (H_3Si)_4-O$	+103	+98
$(HO)_2-Si + HO-OH \rightarrow (HO)_4-Si$	+61	+49
$H_2Si{=}SiH_2 \rightarrow H_3Si-SiH$	+5.1	+4.6
O-bridged $H_2Si-SiH_2 \rightarrow H_2Si-O-SiH_2$ biradical	+28.4	+26.2
O-bridged $H_2Si-SiH_2 \rightarrow O-SiH_2-SiH_2$ biradical	+67.8	+45.3

Table 2 compares the ReaxFF$_{SiO}$ results to the DFT energies for these reactions.

3.5. Reaction Mechanisms. In Si/SiO2 systems, one of the most important reactions is hydrolysis, condensation with H_2O

$$RSiOH + RSiOH \leftrightarrow RSi-O-SiR + H_2O$$

This is important in forming zeolites and plays a role in stress-corrosion cracking of silica glass. To provide data for this process, we carried out DFT and ReaxFF$_{SiO}$ calculations on the reaction of a water molecule with a Si_9H_{10} cluster modeling the (100) surface of Si crystal. Figure 12 shows the energetics for the reactants, reaction product, and various reaction intermediates.

In addition we considered (1) the condensation of two $Si(OH)_4$ clusters to form $(OH)_3Si-O-Si(OH)_3+H_2O$; (2) dehydrocyclization of $HO-SiH_2-O-SiH_2-O-SiH_2-OH$ to form *c*-$(SiH_2O)_3$ ring and H_2O; and (3) Dehydrocyclization of $HO-SiH_2-O-SiH_2-OH$ to form *c*-$(SiH_2O)_2$ ring and H_2O.

The DFT- and ReaxFF$_{SiO}$-results for these are compared in Table 3.

3.6. Crystal Data. Simulations of condensed-phase Si and SiO_2 systems including their interfaces, surface reactions, etc. are key applications for ReaxFF$_{SiO}$. The ability of the ReaxFF$_{SiO}$ potential to predict condensed phase stabilities was tested against

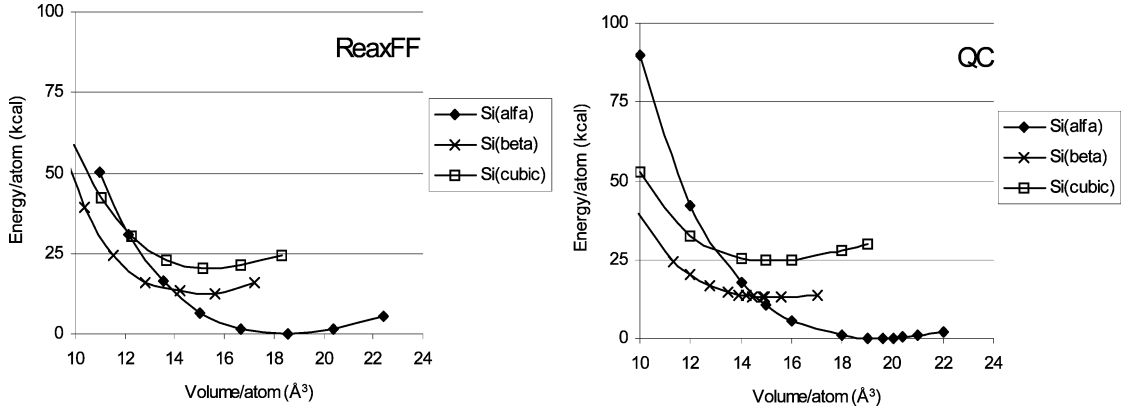

Figure 13. Equation of state (compression and expansion) for three phases of silicon [α is tetrahedral (diamond), β is the 6 coordinate white Sn structure, and cubic is a simple cubic 6 coordinate structure] calculated using ReaxFF and DFT methods.

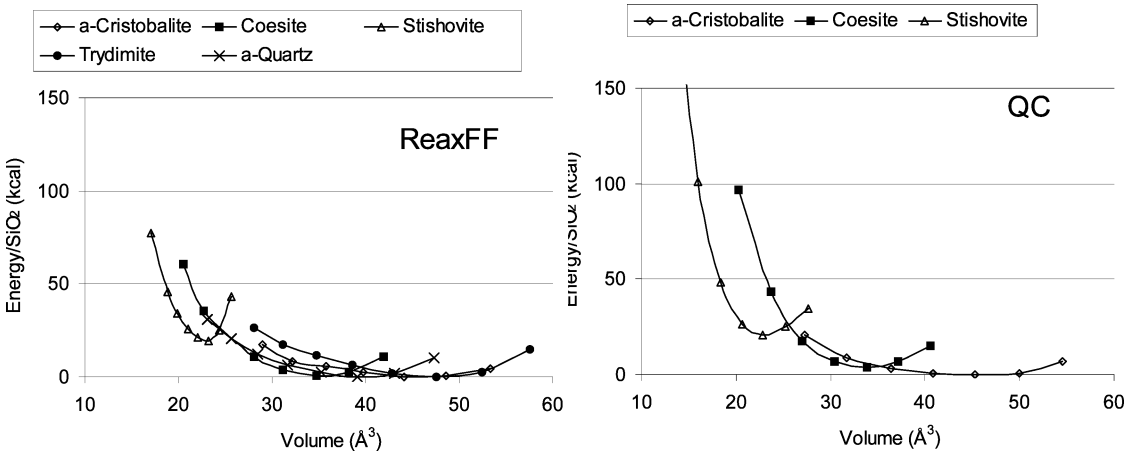

Figure 14. Compression/expansion energies of silicon oxide phases as calculated by the ReaxFF and QC methods. All crystal structures were reminimized after expansion/compression.

TABLE 3: Condensation Reaction Energies (in kcal/mol) as Calculated by DFT and ReaxFF$_{SiO}$

reaction	E_{DFT}	E_{reaxFF}
$Si(OH)_4+Si(OH)_4 \rightarrow$ intermediate	+7.3	+6.4
intermediate $\rightarrow (OH)_3Si-O-Si(OH)_3+H_2O$	−22.3	−22.0
$HO-SiH_2-O-SiH_2-O-SiH_2-OH \rightarrow$ 6-ring$+H_2O$	+11.2	+7.5
$HO-SiH_2-O-SiH_2-OH \rightarrow$ 4-ring$+H_2O$	+34.4	+38.8

TABLE 4: Phase Stabilities (kcal/mol Si) for All-Silicon Systems (Relative to α-Si with the Diamond Structure)

crystal phase/compound	ΔE_{QC}	ΔE_{ReaxFF}
β-Si	13.2	15.2
Si cubic	24.6	20.5
α-Si vacancy	80.2[a]	83.2
Si atom	129.1	128.2

[a] Reference 23.

a variety of crystal structures for silicon and silicon oxides. For each system, the cohesive energy and densities were compared against QC data (Tables 4−6). In addition, for five of these crystal phases, the QC energies were obtained for a broad range of compression and expansion and compared against ReaxFF$_{SiO}$ (Figures13 and 14). We see that ReaxFF correctly describes the equations of state of α, β, and simple cubic Si as well as α-cristobalite, coesite, and stishovite SiO_2.

As the DFT methods applied here to provide QC data to test the force field against do not describe intermolecular forces very well, no specific test cases were generated for the ReaxFF$_{SiO}$ nonbonded potentials. However, the good performance of ReaxFF$_{SiO}$ for these crystal data, and especially the equations

TABLE 5: Silicon Oxide Phase Stabilities (in kcal/mol SiO_2) Relative to α-Quartz

crystal phase	ΔE_{QC}	ΔE_{exp}[a]	ΔE_{ReaxFF}
α-cristobalite	−0.26	0.70	0.06
β-tridymite	−0.25		−0.44
coesite	3.20	0.70	0.42
SSZ-24		1.7	2.9
ZSM-5		2.0	1.4
ZSM-11		2.0	1.4
ZSM-12		2.1	1.5
faujasite		3.3	2.4
stishovite	20.5		19.3
SiO_2 monomer	143.4		125.7

[a] Reference 25.

for state, indicates that ReaxFF$_{SiO}$ provides a good description of van der Waals and Coulomb interactions.

3.7. Charge Distribution. Charge distributions in ReaxFF$_{SiO}$ are calculated using the EEM method.[15] EEM parameters were optimized against Mulliken charge distributions obtained from DFT calculations. In ReaxFF$_{SiO}$, the MD calculations treat Coulomb interactions using a 7th order Taper function,[24] with an outer cutoff radius R_{cut} = 10 Å.

For the $Si(OH)_4$ cluster, the DFT/Mulliken partial charges for the Si, O, and H atoms are +1.054, −0.597, and +0.336, respectively. ReaxFF$_{SiO}$ calculates partial charges for the Si, O, and H atoms of +1.068, −0.620, and +0.353, respectively.

In SiH_4, ReaxFF$_{SiO}$ assigns a partial charge to Si of 0.273, compared to a DFT/Mulliken value of 0.34.

For α-quartz, ReaxFF$_{SiO}$ assigns charges of +1.346 to the Si and −0.673 to the O atoms, which is very similar to the QEq[14]

TABLE 6: Condensed Phase Densities (in kg/dm^3) and Bulk Moduli (in GPa)

crystal	ρ_{ReaxFF}	ρ_{exp}	ρ_{QC}	B_{ReaxFF}[a]	B_{exp}
stishovite	4.29	4.28[b]	4.36	311.5	306−313[d]
coesite	2.95		2.94	67.1	
α-quartz	2.55	2.65[c]		33.4	34−37[e]
α-cristobalite	2.22	2.33[c]	2.20	18.7	15[f]
tridymite	2.09	2.27[c]		21.4	
α-Si	2.50	2.33[c]	2.37	110.0	103[g]
β-Si	2.97		3.11	145.0	
Si cubic	2.79		3.10	160.4	

[a] Determined by fitting the compression/expansion energies of the crystals (Figures 12 and 13) to an equation of state. [b] Reference 26. [c] Reference 27. [d] References 28−30. [e] References 31−33. [f] Reference 34. [g] Reference 35.

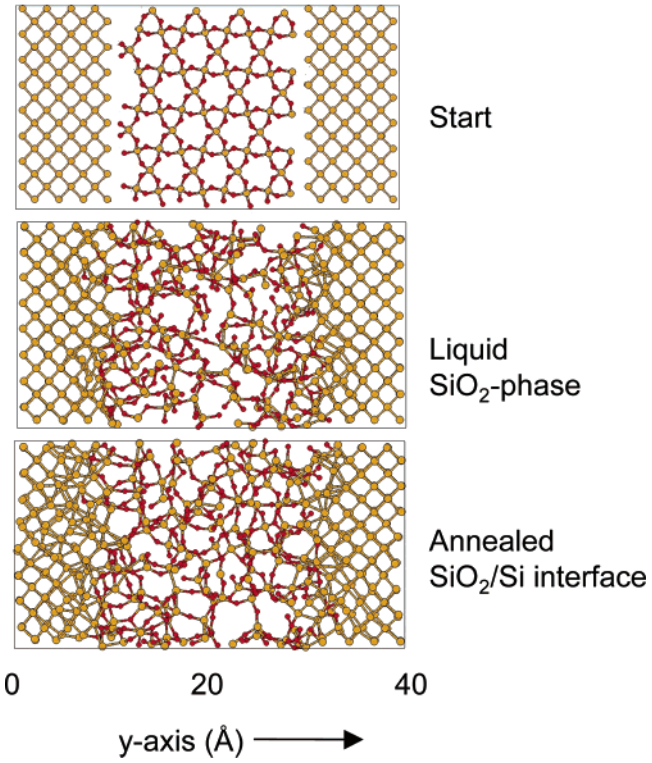

Figure 15. (a) Initial structure (top), (b) structure after melting the α-quartz phase (middle), and (c) final interface structure (bottom).

charge distribution (1.3180 for Si and −0.6590 for O) reported by Demiralp et al.[9]

3.8. Applications. To demonstrate some of the possible applications of ReaxFF$_{SiO}$, we used MD simulations to form the SiO_2/Si interface. We started with a periodic 362-atom slab of α-quartz SiO2 (2.12 by 1.86 by 1.06 nm), sandwiched within a 256-atom slab of α-Si (2.12 by 1.76 by 1.06 nm), as indicated in Figure 15a. These slabs were initially separated by about 1.8 Å. To form an amorphous layer of SiO2 in contact with the crystalline Si, we carried out NVT MD simulations (constant volume and constant temperature using a Berendsen thermostat[36]) using different temperature regimes as follows:

(a) We set the temperature of the Si slab at 100 K with a temperature-damping constant of 2.5 fs, set the temperature of the SiO2 phase at 7000 K with a temperature-damping constant of 50 fs, and carried out 1.75 ps of MD simulations. During this simulation, the quartz melts while the cold α-Si retains its crystalline order (Figure 15b).

(b) Next, we used MD to cool the central region (SiO_2) from 7000 to 300 K in 7.5 ps. During this time, the Si/SiO_2 interface forms (Figure 15c). During the cooling process, we used the same two-thermostat technique used to melt the SiO_2 region, keeping the α-Si region cooled at about 100 K.

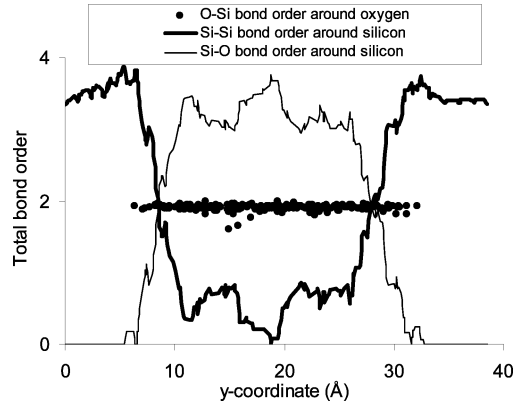

Figure 16. Bond order analysis for the annealed Si/SiO_2 interface.

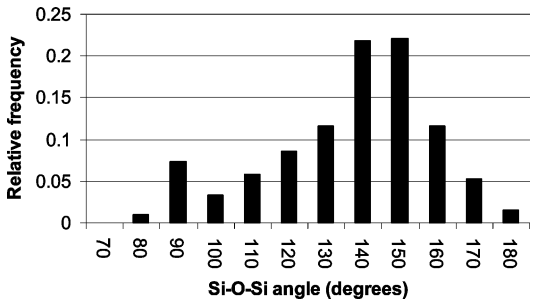

Figure 17. Analysis of the Si−O−Si angles in the annealed Si/SiO_2 interface.

In these simulations, a MD time step of 0.5 fs was used. Atomic charges were updated at every MD iteration. We analyzed the partial bond orders and valence angles in the annealed structure (Figure 15c) and found that all oxygen atoms have a total bond order of 2 to silicon atoms, indicating that no oxygen radicals remain in the system after annealing (Figure 16); no oxygen−oxygen bonds remain in the annealed system; Si−O−Si angle analysis (Figure 17) shows that most of the Si−O−Si angles are in the range of 135 to 170°, but about 10% have angles near 90° indicating some oxygens with 3 silicon neighbors (as in stishovite) even though the total bond order is 2. This shows that most oxygens are two-coordinate; the total bond order at the Si in bulk a-Si is 3.4 and in bulk α-quartz is 3.8. [Figure 16 shows that these values remain about the same with no substantial dip at the interface (4 Si have bond orders as low as 3.2). This indicates that there are no Si radicals in the system.]; the fraction of the Si bonds that are Si−Si bonds drops rapidly (in 5 Å) from 100% to 0%, whereas the fraction that is Si−O increases rapidly (in 5 Å) from 0% to 100% (Figure 16).

These results suggest that ReaxFF$_{SiO}$ creates a credible interface.

Further simulations and more detailed analyses are required to validate these observations by constructing the interface in different ways from a variety of string points. These results can then be compared to full QC results.[37−39] In addition, to validate these results, we must make more detailed comparisons to experimental observations of the interface, and we also plan to perform QC simulations on suitably small interface systems to supply a direct validation of ReaxFF$_{SiO}$. However, the simulations presented here provide a flavor of the possibilities available using ReaxFF$_{SiO}$. This entire simulation took 14 h on a single-processor Compaq XP1000 workstation, demonstrating that

ReaxFF, especially if incorporated in a parallel computing framework, should be able to simulate reactions in very large systems.

4. Discussion

As discussed by Kramer et al.,[3] there is a distinct difference between hydrocarbons force fields and silica force fields. Most hydrocarbon force fields employ an intricate potential function scheme,[40−42] using various partial energy contributions and a large number of parameters, but silica force fields tend to use far fewer terms with only a limited number of parameters. Furthermore, hydrocarbon force fields tend to be strictly covalent, whereas silica force fields are sometimes either completely ionic or partially ionic.

As demonstrated by the success of generic force fields such as DREIDING[43] or UFF,[44] there is no direct reason for these fundamental differences between hydrocarbon and silica force field design. Electronegativity equalization and charge equilibration schemes[14,15] which have been successfully applied to both hydrocarbons[16,17] and silica[5,9] force fields help to bridge the gap between covalent and borderline ionic systems, allowing similar potential functions to capture the remaining non-Coulombic interactions. This is demonstrated by the good agreement between the QC and the $ReaxFF_{SiO}$ data presented in this work. The biggest deviations from the QC data (e.g., the location of the Si═O equilibrium bond length in Figure 6; and the crystal densities in Table 6) arise because the force field systematically predicts a somewhat lower density for the silicon oxide phases than experiment. This is primarily due to compromises made to fit both the cluster and the condensed phase data with a single force field. Neither of these deviations are serious, and the general quality of the fit between QC and $ReaxFF_{SiO}$ combined with the scope of silicon chemistry covered by the QC-based training set indicate that $ReaxFF_{SiO}$ should have a broad range of applications.

To facilitate future force field development, we chose to employ all of the partial energy functions used in $ReaxFF_{CH}$ also for $ReaxFF_{SiO}$. The instability of the Si−Si double bond (Figures 3−4), however, makes several partial energy contributions virtually negligible in $ReaxFF_{SiO}$. Obvious examples of these are the conjugation and penalty energy (E_{conj} and E_{pen}, eq 1), which are directly related to a certain amount of π-bond order. Furthermore, torsion energy contributions are practically zero, indicating that in silicon σ-bonded systems rotation barriers can be described by nonbonded interactions. This seems to be in agreement with findings by Pophristic and Goodman,[45] who found that in disilane the rotational barrier is much reduced compared to that in ethane. If we were to target the reactive force field exclusively at silicon and silicon oxide systems, these partial energy contributions could be removed from the force field, generating a force description not much more complicated than that of most empirical silica force fields.

5. Conclusions

We have developed the $ReaxFF_{SiO}$ reactive force field for silicon and silicon oxide systems based on the $ReaxFF_{CH}$ reactive force field for hydrocarbons.[16] $ReaxFF_{SiO}$ has been tested against a substantial data set derived from quantum chemical calculations on small clusters and on condensed systems and covering both reactive and nonreactive aspects of silicon oxides. The good agreement between the QC and $ReaxFF_{SiO}$ results for these systems indicates that the $ReaxFF_{SiO}$ can be used to simulate aspects of silicon oxide reactivity opening up new possibilities for the role of computational chemistry in materials sciences.

Acknowledgment. This research was supported by a Royal Society Fellowship (ACTvD) and by support from Seiko-Epson (Mr. Uehara and Dr. Miyata). The facilities of the MSC used in this work are supported by grants from DOE-ASCI, ARO/DURIP, ARO/MURI, NIH, NSF, Chevron, Beckman Institute, 3M, Dow Chemical, Avery-Dennison, and Asahi Chemical.

TABLE A1: General Parameters[a]

parameter	value	description
λ_1	50.0	overcoordination bond order correction
λ_2	5.55	overcoordination bond order correction
λ_3		in atom parameters (p_{131}; Table A3)
λ_4		in atom parameters (p_{132}; Table A3)
λ_5		in atom parameters (p_{133}; Table A3)
λ_6		in atom parameters ($p_{ov/un}$; Table A2)
λ_7	1.02	undercoordination energy
λ_8	−6.32	undercoordination energy
λ_9	13.02	undercoordination energy
λ_{10}		in atom parameters ($p_{ov/un}$; Table A2)
λ_{11}		in atom parameters ($p_{v,3}$; Table A2)
λ_{12}		in valence angle parameters ($p_{v,4}$; Table A7)
λ_{13}		in atom parameters ($p_{v,5}$; Table A2)
λ_{14}		in atom parameters ($p_{v,6}$; Table A2)
λ_{15}	33.87	valence angle energy
λ_{16}	25.6	lone pair parameter (eq 5)
λ_{17}	1.06	valence angle energy
λ_{18}	2.04	valence angle energy
λ_{19}		in valence angle parameters (p_{pen}; Table A7)
λ_{20}	6.93	penalty energy
λ_{21}	0.40	penalty energy
λ_{22}	4.00	penalty energy
λ_{23}	4.77	torsion energy
λ_{24}	10.00	torsion energy
λ_{25}	2.33	torsion energy
λ_{26}		in torsion angle parameters (p_{conj}; Table A8)
λ_{27}	2.16	conjugation energy
λ_{28}	1.559	van der Waals energy
λ_{32}	1.63	lone pair/overcoordination (eq 6b)
λ_{33}	5.69	lone pair/overcoordination (eq 6b)

[a] As noted, some of the parameters designated in $ReaxFF_{CH}$ as general have been moved elsewhere in the force field.

TABLE A2: Atom Parameters (p_{over} in kcal/mol)

atom	$p_{ov/un}$	p_{under}	$p_{v,3}$[a]	$p_{v,5}$[a]	$p_{v,6}$[a]
Si	−3.7	11.4	3.19	6.30	2.58
O	−7.3	39.3	2.67	6.30	2.92
H	−12.6	0	2.99	6.30	2.58

[a] Used for all valence angles with this atom in a central position.

TABLE A3: Coulomb and 1−3 Bond Order Correction Parameters

	Coulomb parameters			1−3 BO correction		
atom	η (eV)	χ (eV)	γ (Å)	λ_3	λ_4	λ_4
Si	1.80	7.39	0.82	6.23	5.23	0.15
O	7.83	8.5	1.08	6.58	4.31	1.00
H	9.88	3.82	0.76	4.07	2.69	1.00

TABLE A4: van der Waals and Bond Radius Parameters

atoms	r^{σ} Å	r^{π} Å	r_{vdW} Å	ee kcal/mol	aa	γ_w Å
Si−Si	2.013	1.563	4.441	0.131	12.13	1.88
Si−O	1.610	1.294	3.510	0.123	10.69	3.69
O−O	1.169	1.020	3.916	0.088	10.18	7.25
O−H	0.912		3.601	0.045	10.13	5.53
Si−H	1.193		3.109	0.045	12.48	2.80
H−H	0.656		3.312	0.023	10.08	4.16

TABLE A5: Bond Energy Parameters (D_e^{σ}, D_e^{π}, and $D_e^{\pi\pi}$ in kcal/mol)

bond	D_e^{σ}	D_e^{π}	$D_e^{\pi\pi}$	$p_{be,1}$	$p_{be,2}$	$p_{be,3}$
Si−Si	113.8	54.0	0	0.25	0.26	0.07
Si−O	193.1	41.1	0	−0.21	0.92	0.77
Si−H	138.9			−0.16	17.9	0.29
O−O	118.9	42.8		0.91	0.86	0.86
O−H	199.5			−0.91	3.02	0.59

TABLE A6: Bond Order Parameters

bond	$p_{bo,1}$	$p_{bo,2}$	$p_{bo,3}$	$p_{bo,4}$	$p_{bo,5}$	$p_{bo,6}$
Si−Si	−0.069	7.94	−0.20	7.54		
Si−O	−0.519	4.45	−0.37	4.26		
Si−H	−0.040	6.39				
O−O	−0.161	5.66	−0.25	6.52	−0.16	10.51
O−H	−0.044	5.26				

TABLE A7: Valence Angle Parameters

angle	$\Theta\Theta_{o,o}$	k_a	k_b	$p_{v,1}$	$p_{v,2}$	$p_{v,4}$	p_{pen}
Si−Si−Si	69.3[a]	21.7	1.4	0	−0.2	1.32	0
Si−Si−O	70.3	15.4	1.3	0	2.1	1.04	0
O−Si−O	90.0	7.8	1.7	0	0.8	1.04	0
H−Si−Si	75.6	21.5	1.0	0	2.5	1.04	0
H−Si−O	73.8	16.7	3.7	0	0.9	1.04	0
H−Si−H	78.4	21.0	0.9	0	2.8	1.04	0
O−O−O	78.5	61.0	1.0	0	0.5	1.04	0
Si−O−O	73.5	25.1	0.9	0	2.2	1.04	0
Si−O−Si	22.2	3.7	0.3	0	4.1	1.04	0
H−O−Si	83.8	5.7	2.8	0	1.7	1.04	0
H−O−O	89.5	10.1	4.8	0	0.0	1.04	0
H−O−H	81.7	15.4	1.2	0	0.0	1.04	0
H−H−H	0	27.9	6.0	0	0.0	1.04	0
H−H−Si	0	47.1	6.0	0	1.6	1.04	0
Si−H−Si	0	31.5	6.0	0	1.6	1.04	0
H−H−O	0	0.0	6.0	0	0.0	1.04	0
O−H−O	0	0.0	6.0	0	0.0	1.04	0
O−H−Si	0	31.0	6.0	0	1.6	1.04	0

[a] This value leads to an equilibrium angle of 180−69.3 = 110.7° for the single bond Si−Si−Si valence angle.

TABLE A8: Torsion Angle Parameters (V_1, V_2, and V_3 in kcal/mol)[a]

torsion angle	V_1	V_2	V_3	p_t	p_{conj}
Si−Si−Si−Si	0	0	0.0	−2.40	0
X−Si−O−X[b]	0	0	0.0	−2.40	0
X−O−O-X[c]	2.6	−1.7	2.6	−4.7	−1.23
H−Si−Si−Si	0	0	0.16	−2.40	0
H−Si−Si−H	0	0	0.06	−2.40	0

[a] Torsion angles not defined in this table (i.e., C−H−C−C) are assigned torsion barrier energies of 0 kcal/mol. [b] Used for all torsion angles with a central Si−O bond. [c] Used for all torsion angles with a central O−O bond.

References and Notes

(1) Sander, M. J.; Leslie, M.; Catlow, C. R. A. *J. Chem. Soc. Chem. Commun.* **1984**, 1271.

(2) Tsuneyuki, S.; Tsukada, M.; Aoki, H.; Matsui, Y. *Phys. Rev. Lett.* **1988**, *61*, 869.

(3) Kramer, G. J.; Farragher, N. P.; van Beest, B. W. H.; van Santen, R. A. *Phys. Rev. B* **1991**, *43*, 5068.

(4) Nicholas, J. B.; Hopfinger, A. J.; Trouw, F. R.; Iton, L. E. *J. Am. Chem. Soc.* **1991**, *113*, 4792−4800.

(5) Burchart, E. D.; Verheij, V. A.; van Bekkum, H.; van de Graaf, B. *Zeolites* **1992**, *12*, 183.

(6) Belonoshko, A. B.; Dubrovinsky, L. S. *Geochim. Cosmochim. Acta* **1995**, *59*, 1883.

(7) Ermoshin, V. A.; Smirnov, K. S.; Bougeard, D. *Chem. Phys.* **1996**, *202*, 53−61.

(8) Blake, N. P.; Weakliem, P. C.; Metiu, H. *J. Phys. Chem. B* **1998**, *102*, 67.

(9) Demiralp, E.; Cagin, T.; Goddard, W. A. *Phys. Rev. Lett.* **1999**, *82*, 1708.

(10) Tsuneyuki, S.; Matsui, Y.; Aoki, H. *Nature* **1989**, *339*, 209.

(11) Geidel, E.; Bohlig, H.; Birner, P. *Z. Phys. Chem.* **1991**, *171*, 121.

(12) Smirnov, K. S.; Thibault-Starzyk, F. *J. Phys. Chem. B* **1999**, *103*, 8595.

(13) Ermoshin, V. A.; Engel, V. *J. Phys. Chem. A* **1999**, *103*, 5116.

(14) Rappé, A. K.; Goddard, W. A. *J. Phys. Chem.* **1991**, *95*, 3358.

(15) Mortier, W. J.; Ghosh, S. K.; Shankar, S. J. *J. Am. Chem. Soc.* **1986**, *108*, 4315.

(16) van Duin, A. C. T.; Dasgupta, S.; Lorant, F.; Goddard, W. A. *J. Phys. Chem. A* **2001**, *105*, 9396.

(17) Payne, M. C.; Teter, M. P.; Allan, D. C.; Arias, T. A.; Joannopoulos, J. D. *Rev. Mod. Phys.* **1992**, *64* 1045.

(18) Perdew, J. P.; Burke, K.; Ernserhof, M. *Phys. Rev. Lett*. **1996**, *77*, 3865.

(19) Monkhorst, H. J.; Pack, J. D. *Phys. Rev. B* **1976**, *13*, 5188.

(20) Perdew, J. P.; Wang, Y. *Phys. Rev. B* **1992**, *46*, 6671.

(21) van Duin, A. C. T.; Baas, J. M. A.; van de Graaf, B. *J. Chem. Soc., Faraday Trans.* **1994**, *90*, 2881.

(22) See our web-site http://www.wag.caltech.edu/publications/papers/.

(23) Hwang, G. S.; Goddard, W. A. III. *Phys. Rev. B* To be published.

(24) de Vos Burchart, E. *Studies on Zeolites: Molecular Mechanics, Framework Stability, and Crystal Growth*. Ph.D. Thesis, Delft University of Technology, Delft, The Netherlands, 1992.

(25) Navrotsky, A. *Rev. Mineral.* **1994**, *29*, 309.

(26) Spackman, M. A.; Hill, R. J.; Gibbs, G. V. *Phys. Chem. Minerals* **1987**, *14*, 139.

(27) *Handbook of Chemistry and Physics 2000/2001*; CRC Press: Boca Raton, FL, 2001.

(28) Liu, L. G.; Bassett, W. A.; Takahashi, T. *J. Geophys. Res.* **1974**, *79*, 1160.

(29) Bassett, W. A.; Barnett, J. D. *Phys. Earth Planet. Inter.* **1970**, *3*, 54.

(30) Tsuchida, Y.; Yagi, T. *Nature (London)* **1989**, *340*, 217.

(31) Levien, L.; Prewitt, C. T.; Weidner, D. J. *Am. Mineralog.* **1980**, *65*, 920.

(32) Glinnemann, J.; King, H. E., Jr.; Schulz, H.; Hahn, Th.; Laplaca, S. J.; Dacol, F. *Z. Kris.* **1992**, *198*, 177.

(33) Hazen, R. M.; Finger, L. W.; Hemley, R. J.; Mao, H. K. *Solid State Commun.* **1989**, *72*, 507.

(34) Liu, F.; Garofalini, S. H.; King-Smith, D.; Vanderbilt, D. *Phys. Rev. B* **1994**, *49*, 12528.

(35) Rignanese, G.-M.; Michenaud, J.-P.; Gonze, X. *Phys. Rev. B* **1996**, *53*, 4488.

(36) Berendsen, H. J. C.; Postma, J. P. M.; van Gunsteren, W. F. *J. Chem. Phys.* **1984**, *81*, 3684.

(37) Chu, A. X.; Beall Fowler, W. *Phys. Rev. B* **1990**, *41*, 5061.

(38) Pasquarello, A.; Hybertsen, M. S.; Car, R *Phys. Rev. Lett.* **1995**, *74*, 1024.

(39) Yamasaki, T.; Kaneta, C.; Uchiyama, T.; Uda, T.; Terakura, K. *Phys. Rev. B* **2001**, *63*, 115314.

(40) Allinger, N. L.; Yuh, Y. H.; Lii, J.-H. *J. Am. Chem. Soc.* **1989**, *111*, 8551.

(41) Maple, J. R.; Hwang, M.-J.; Stockfish, T. P.; Dinur, U.; Waldman, M.; Ewig, C. S.; Hagler, A. T. *J. Comput. Chem.* **1994**, *15*, 162.

(42) Dillen, J. L. M. *J. Comput. Chem.* **1990**, *11*, 1125.

(43) Mayo, S. L.; Olafson, B. D.; Goddard, W. A. *J. Phys. Chem.* **1990**, *94*, 868.

(44) Rappé, A. K.; Casewit, C. J.; Colwell, K. S.; Goddard, W. A.; Skiff, W. M. *J. Am. Chem. Soc.* **1992**, *114*, 10024.

(45) Pophristic, V.; Goodman, L *J. Chem. Phys.* **2001**, *115*, 5132.